

Study of a Family of 40 Hydroxylated β -Cristobalite Surfaces Using Empirical Potential Energy Functions

Shikha Nangia,[†] Nancy M. Washton,[†] Karl T. Mueller,[†] James D. Kubicki,[‡] and Barbara J. Garrison^{*,†}

104 Chemistry Building, Department of Chemistry, Department of Geosciences and The Earth and Environmental Systems Institute, The Pennsylvania State University, University Park, Pennsylvania 16802

Received: November 27, 2006; In Final Form: January 31, 2007

We present a study of a family of 40 unique hydroxylated β -cristobalite surfaces generated by cleaving the β -cristobalite unit cell along crystallographic planes to include a combination of several low Miller index surfaces. The surface silicon atoms are quantified as percentages of Q² and Q³ centers based on their polymeric state. We find that Q³ centers are, on average, three times more abundant than Q² centers. To study the surface properties, we use two different empirical potential energy functions: the multibody potential proposed by Fueston and Garofalini (*J. Phys. Chem.* **1990**, *94*, 5351) and the newly developed CHARMM potential by Lopes et al. (*J. Phys. Chem. B* **2006**, *110*, 2782). Our results for the surface water interactions are in good agreement with previous ab initio theoretical studies by Yang et al. (*Phys. Rev. B* **2006**, *73*, 146102) for the (100) surface. We find that the most commonly studied family of {100} surfaces is unique and is the only surface with 100% abundance of Q² centers, whereas there are nine examples of surfaces with 100% Q³ centers. The predominantly pure Q³ surfaces show no hydrogen bonding with the neighboring surface hydroxyl groups and weakly adsorb water overlayers. This is markedly different from the {100} pure Q² surface that shows strong hydrogen bonding within the surface groups and with water. As compared to all the surfaces studied in this work, we find that the {100} surfaces are not true representations of the overall β -cristobalite surfaces and their properties. We find that the two main factors that characterize the physical properties of silica surfaces are the polymeric state of the silicon atom and surface topography. Two types of pure Q³ crystallographic planes have been identified and are labeled as Q^{3A} and Q^{3B} based on the differences in their topological features. Using the {111} and {011} surfaces as examples, we show that the Q^{3A} surface adsorbs H₂O that forms a stable monolayer, but the Q^{3B} surface fails to form a stable H₂O overlayer. Other crystallographic planes with different ratios of Q² to Q³ centers are contrasted by the differences in the hydrogen-bonding network and their ability to form ordered H₂O overlayers.

I. Introduction

Silica (SiO₂) with its myriad industrial uses and ubiquitous presence in nature is necessarily one of the most studied oxide surfaces in both crystalline and amorphous forms.^{1–7} Silica surfaces are relevant in studies of glass corrosion, self-assembled monolayers, processing silicon semiconductors, and human health to name a few examples. Recent work has demonstrated that oxide surface properties can vary dramatically from crystal face to crystal face.⁸ Hence, it is necessary to have a reasonably efficient method for mapping out all the potential crystal faces of an oxide particle and predicting their surface chemistries. Experiments and electronic structure calculations can then focus on the most representative crystal faces, and the behavior of the particle can be determined based on summation of all the contributing facets.

Silica is also an environmentally relevant mineral. Dissolution of silica during the weathering of rocks is an important component of the global carbon cycle and thus affects predictions of future climate change related to increasing greenhouse

gas concentration in the Earth's atmosphere (i.e., global warming). Although there have been advances in this field, the microscopic details of silica dissolution are yet to be understood completely. Dissolution occurs at the silica–water interface at which the hydroxylated surfaces can undergo hydrolysis catalyzed by hydronium or hydroxide ions.^{9,10} These studies have not taken into account, however, the long-range structure of the large variety of silica surfaces and the effect this structure has on the interaction with water. From studies on α -TiO₂,^{11–13} oxide–water interfaces can vary significantly from crystal face to crystal face. These differences affect the isoelectric point of the crystal faces¹⁴ that strongly influences the sorption behavior of the surface. Adsorption is another important environmental process in the transport of toxic metals and agro-chemicals in soils and groundwater.^{15,16} Considering these variations, a more general view of possibilities for the silica–water interface is warranted. Silica surfaces with different topologies can also result in different dissolution and adsorption properties.^{17–21} Gratz et al.¹⁹ have shown that the rate of dissolution can differ by an order of magnitude depending on the organization of surface into steps (roughness) or straightening of steps (smoothness).

Another area where silica–water interactions are important is human health. The relationship of surface properties of

* To whom correspondence should be addressed. E-mail: bjg@psu.edu.

[†] Department of Chemistry.

[‡] Department of Geosciences and The Earth and Environmental Systems Institute.

TABLE 1: Percentage of Q³ Centers of the 40 β -Cristobalite Surfaces Arranged in Descending Order^a

surface Miller index	% Q ³	surface Miller index	% Q ³
{111}	100(A)	{134}	86
{011}	100(B)	{135}	86
{122}	100(AB)	{234}	86
{133}	100(AB)	{034}	85
{144}	100(AB)	{123}	78
{155}	100(AB)	{023}	75
{334}	100(A)	{035}	75
{355}	100(A)	{113}	75
{445}	100(A)	{235}	73
{255}	95	{225}	71
{214}	95	{012}	67
{045}	94	{112}	67
{344}	93	{115}	67
{233}	91	{114}	56
{145}	89	{025}	54
{223}	89	{125}	54
{455}	89	{013}	50
{335}	88	{014}	38
{345}	88	{015}	36
{245}	87	{100}	0

^a The letters A and B in parentheses in the % Q³ column denote the type of topology of the surface. The percentage of Q² centers is calculated as (100 - % Q³) for each surface.

TABLE 2: Calculated Bond Lengths (Å) and Bond Angles (in Degrees) for β -Cristobalite Using the FG Potential

	experiment ^a	ref 39	this work
lattice parameter <i>a</i>	7.16	7.21	7.18
Si–O	1.611	1.612	1.64
Si–O–Si	107.8, 112.8	109.4, 110.2	108.7, 111.2
O–Si–O	146.6	150.9, 178.5	152.3, 154.7

^a Ref 61.

crystalline heat-treated cristobalite has been studied experimentally to understand the micromorphology of the surfaces and their toxicity to living tissue.²² Fubini et al.²² presented data of the adsorption of water vapor on cristobalite at several temperatures. The enthalpy of water adsorption onto cristobalite is related to the relative toxicity of the particles.²² Knowledge of how water will interact with various faces is thus critical in developing a molecular-level understanding of silica toxicity in lungs.

The chemical properties and reactivity of the surface depend on the polymeric state of the silicon center at the surface and the topology.^{23,24} Polymerization of silicate tetrahedra (SiO₄⁴⁻) is classified using the Q^{*i*} notation, where *i* is equal to the number of bridging oxygen atoms (O_{br}) connected to the Si center; the remaining bonds are typically terminated with hydroxyl groups.^{25–28} For example, β -cristobalite surfaces mainly contain Q² and Q³ centers, which have two and three O_{br}, and two and one hydroxyl terminations, respectively.

Qualitative and quantitative assessments of the hydroxyl groups on silica have been experimentally performed using ²⁹Si nuclear magnetic resonance (NMR),^{29–32} infrared radiation (IR),^{33–35} and X-ray reflectivity.³⁶ NMR spectroscopy can distinguish between the Q² and Q³ centers, and it was found that on silica gels Q² centers are less abundant on the surface than Q³ species and range between 15–30% on an average of the total surface species.^{29,30,32} IR spectroscopy on silica gels provides insight into the hydrogen-bonding (H-bonding) properties of the hydroxyls by identifying the distribution of hydroxyl groups,^{33–35} while X-ray reflectivity techniques have been used to elucidate the structural and energetic properties of the surface water interface. Using the X-ray reflectivity technique on (10 $\bar{1}$ 0) and (10 $\bar{1}$ 1) quartz surfaces, Schlegel et al.³⁶

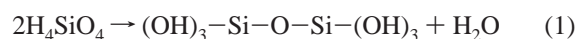
have shown that morphologically flat crystal surfaces adsorb only a single layer of water (monolayer) with no further structure beyond the monolayer, whereas corrugated surfaces have a disordered and random distribution of adsorbed H₂O molecules.²²

The main factors influencing the H-bonding on a silica surface are the type of Si center(s) involved, the distance between the surface hydroxyls, and the orientation of the hydroxyl groups. If all hydroxyl groups lie within the same plane parallel to the surface, then H-bonding is facilitated between the adjacent Si centers. Using density functional theory and molecular dynamics (MD) simulations, it has been shown that water adsorbs on the (100) silica surface and forms an ordered icelike network, a process referred to as tessellation.^{37–39}

The most commonly investigated polymorphs of silica are α ,(β)-quartz and cristobalite because of their comparable refractive indices and density to amorphous silicates for which experimental data are available.^{38–40} So far, computational studies of surfaces have concentrated on a small set of crystallographic planes, such as the (100), (111), and (011) planes of α ,(β)-quartz and cristobalite, and the (0001) plane of quartz.^{38,39,41} Both quartz and cristobalite have no preferred crystallographic cleavage plane,⁴² and therefore powdered or crushed samples of these silicates will have a complex structure, presumably composed of some combination of low index Miller planes.

The motivation of the present work is to use efficient computational techniques to study and analyze a large set of surfaces and investigate surface topologies, so that a more comprehensive picture of the surface of crushed β -cristobalite grains can be achieved. On the basis of the topology, it is also interesting to investigate the role of H-bonding between the surface hydroxyl groups and adsorbed water overlayers. In the present work, the MD method was chosen to obviate the computational expense of ab initio methodology, and here we also compare the results from two disparate potential energy functions. These potential energy functions are a key component of MD simulations and are used to describe molecular motion for the chemical system under study.

Although describing all interactions and microscopic behavior in functional form is inherently difficult and complex, analytical force fields have been proposed and parametrized to describe systems such as the silica–water interface (i.e., the hydroxyl groups in aqueous media).^{43,44} In this work, we utilize the potential energy function proposed by Feuston and Garofalini (FG) in 1990.⁴⁵ It is a reactive potential and has been used in various applications to describe H₂O–H₂O, H₂O–H₄SiO₄, H₂O–H₆Si₂O₇, and H₄SiO₄–H₄SiO₄ interactions in aqueous media.^{46–48} By using the FG potential, it has been shown that the polymerization of silicic acid leads to the formation of cyclic structures by first forming linear condensation products



The reaction proceeds through the formation of a pentacoordinated intermediate, and the activation energy achieved computationally for the reaction is in good agreement with experiments.⁴⁸ Along with reactions, the FG potential also describes the H-bonding patterns in dimeric and polymeric structures of water and between water and a silica surface.^{37–39} The potential is well suited for our work, as it provides a description for several key interactions for surface silica–water chemistry.

In a more recent paper, the FG potential was used to study hydrophilic wafer bonding on amorphous silica surfaces in which the hydroxylated surfaces in the presence of water molecules lead to the formation of Si–O–Si bridges across the interface.⁴⁹ A main advantage of the FG potential is that it is able to treat the O and H atoms (in hydroxyl groups) bonded to the surface as well as the O and H atoms of the adsorbed water molecules on the surface using the two-body and three-body interactions terms in its functional form.

The second potential energy function used in the present work is the Chemistry at Harvard Molecular Mechanics (CHARMM) empirical force field.^{50,51} Although incapable of describing bond-breaking and bond-making processes, it is applicable for the study of nonreactive systems and has been used extensively for the study of proteins, nucleic acids, lipids, and carbohydrates,^{52–54} and more recently it has been used for studies of the surface of silica.⁴¹ The potential was parametrized to study the H-bonding network of water in the vicinity of silica surfaces and was shown to have good agreement with the experimental structure of water on quartz.¹¹

II. Potential Energy Functions

For the MD calculations, we use the FG and CHARMM potentials to describe the silica–water interactions. The FG potential energy function is a sum of modified Born–Mayer–Huggins (two-body) term, modified Stillinger and Weber (three body) term,⁵⁵ and a modified Rahman–Stillinger–Lemberg potential.⁵⁶ The functional form is

$$V_{\text{FG}} = V_{ij}^{(2)} + V_{jik}^{(3)} \quad (2)$$

where $V_{ij}^{(2)}$ and $V_{jik}^{(3)}$ are the two-body and three-body interaction terms, respectively. More specifically, the $V_{ij}^{(2)}$ term between atom i and j is

$$V_{ij}^{(2)} = A_{ij} e^{(-r_{ij}/\rho_{ij})} + \frac{q_i q_j}{4\pi\epsilon_o r_{ij}} \operatorname{erfc}\left(\frac{r_{ij}}{\beta_{ij}}\right) + \frac{a_{ij}}{1 + e^{(b_{ij}(r_{ij}-c_{ij}))}} \quad (3)$$

where r_{ij} is the internuclear distance between atoms i and j , q_i is the formal charge on atom i , ϵ_o is the permittivity of free space, and A_{ij} , β_{ij} , ρ_{ij} , a_{ij} , b_{ij} , and c_{ij} are adjustable parameters, provided elsewhere.^{45,49} The $V_{jik}^{(3)}$ term is

$$V_{jik}^{(3)} = \begin{cases} \lambda_{ijk} \{ \cos(\theta_{jik}) - \cos(\theta_{jik}^0) \}^2 \exp\left(\frac{\gamma_{ij}}{r_{ij} - r_{ij}^0} + \frac{\gamma_{ik}}{r_{ik} - r_{ik}^0}\right) & \text{for } r_{ij} < r_{ij}^0 \text{ and } r_{ik} < r_{ik}^0 \\ 0 & \text{otherwise} \end{cases} \quad (4)$$

with θ_{jik} as the angle subtended by r_{ij} and r_{ik} with i being the vertex atom and λ_{ijk} , γ_{ij} , γ_{ik} , θ_{jik}^0 , r_{ij}^0 , and r_{ik}^0 are adjustable parameters, provided elsewhere.^{45,49} For a given atom, a cutoff distance of 5.5 Å was used to calculate all forces. Note that we used the corrected parameters for our calculations and took into account the typographical error mentioned in the literature.⁴⁹

Recently, Lopes et al. developed a CHARMM potential for silica capable of describing the silica–water interactions.⁴¹ The potential energy function is pairwise additive and is written as sum of bonded and nonbonded interaction terms

$$V = V_b + V_{\text{nb}} \quad (5)$$

The V_b term is further written as

$$V_b = \sum_{\text{bonds}} k_b (b - b_0)^2 + \sum_{\text{UB}} k_{\text{UB}} (S - S_0)^2 + \sum_{\text{angles}} k_\theta (\theta - \theta_0)^2 + \sum_{\text{impropers}} k_{\text{imp}} (\varphi - \varphi_0)^2 + \sum_{\text{dihedrals}} k_\chi (1 + \cos(n\chi - \delta)) \quad (6)$$

a sum over the bond (b), Urey–Bradley (S), angle (θ), improper (φ), and dihedral angle (χ) interaction terms, where b_0 , S_0 , θ_0 , and φ_0 are the equilibrium bond distance, 1–3 distance, angle, and improper angle, respectively, and k_b , k_{UB} , k_θ , and k_{imp} are the corresponding force constants. In the last term k_χ , n , and δ are the dihedral force constant, multiplicity, and phase angle, respectively.

The V_{nb} term is a sum over all the nonbonded interactions and is applied to atom pairs that are separated by a minimum of three atoms

$$V_{\text{nb}} = \sum_{\text{nb-pairs}} \left[\frac{q_i q_j}{4\pi\epsilon_o r_{ij}} - \epsilon_{ij} \left\{ \left(\frac{R_{\text{min},ij}}{r_{ij}} \right)^{12} - 2 \left(\frac{R_{\text{min},ij}}{r_{ij}} \right)^6 \right\} \right] \quad (7)$$

The first term is the electrostatic interaction between atoms i and j with partial atomic charge q_i and q_j , internuclear distance r_{ij} , and the second term is the Lennard-Jones function with minimum interaction radius $R_{\text{min},ij}$, and well-depth parameter ϵ_{ij} .

The parameter set for MD simulations was calibrated against experimental and quantum mechanical results for a small set of model compounds. The atoms in a system are grouped into atom types based on several criteria, including hybridization, aliphatic or aromatic neighbors, and oxidation state.

III. Computational Details

The β -cristobalite surfaces were generated using the surface generation module in Cerius² software.⁵⁷ The process of generating surfaces was automated by cleaving the β -cristobalite unit cell into the 40 desired crystallographic planes. It is important to note that the cleavage process in the Cerius² software can be nonunique if the cleavage boundary is manually translated to change the number of bonds broken per SiO₄ tetrahedron. In this work, we used the default settings in the software with no manual intervention to keep the cleavage procedure consistent and reproducible. The unsaturated dangling bonds on the surfaces were hydroxylated. The β -cristobalite structure has a cubic face-centered lattice with symmetry space group $Fd3m$ and unit cell dimensions $a = b = c = 7.16$ Å, and angles $\alpha = \beta = \gamma = 90^\circ$. The cubic symmetry of the lattice makes the crystal axes symmetric and the crystallographic planes equivalent (i.e., (100) \equiv (010) \equiv (001)), and by virtue of symmetry the family of planes is collectively written as {100} planes.⁵⁸ We will follow this notation for the surfaces studied in this paper. We generated a range of { hkl } surfaces with all permutations of Miller indices varying from 0 to 5. The surface area of each slab was approximately 30×30 Å² with a thickness of 15 Å comprising of 7–9 atomic layers and an average of 950 atoms.

The calculations were carried out using the CHARMM software.⁵⁰ We used the USERSB hook utility provided in the CHARMM software to incorporate the FG potential and its analytic derivatives as a user-defined routine. For the calculations using the CHARMM potential, we defined each slab as a separate residue and assigned parameters to each atom in the

TABLE 3: Calculated OO Distances (in Å) for {100}, {111}, and {011} β -Cristobalite Surfaces, Using the CHARMM and FG Potentials

surface	OO distances (Å)	
	CHARMM	FG
{100}	2.8	2.7
{111}	5.1	5.2
{011}	4.2, 5.0	4.3, 5.2

TABLE 4: Average H-bond Distances (Å) for the β -Cristobalite Surfaces and Adsorbed Water and Percentage of the Number of H-Bonds Per Surface Hydroxyl Group Obtained Using the FG Potential

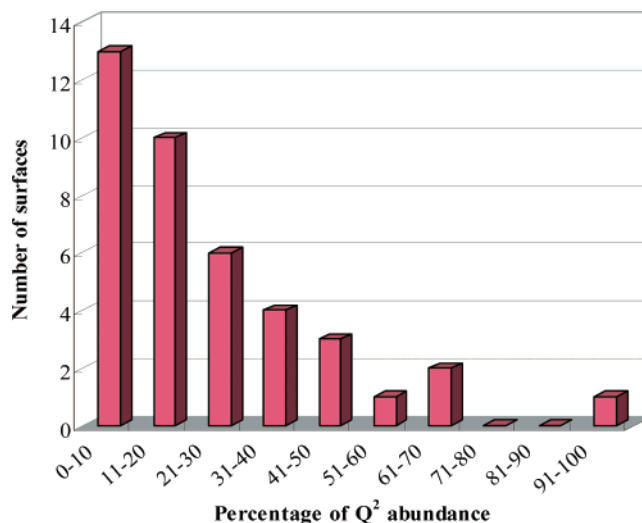
surface	average O–H distance (Å)	percentage of H-bonds/hydroxyl
{035}	2.35	10
{235}	2.31	10
{225}	2.31	18
{025}	2.24	20
{112}	2.18	25
{125}	2.18	25
{014}	2.29	28
{013}	2.27	30
{114}	2.30	30
{115}	2.23	33
{012}	2.19	50
{015}	2.20	50
{113}	2.18	66
{100}	2.01	100

slab based on the atom types provided by the recently developed parameter set for silica, and the TIP3P parameter set⁵⁹ was used for water. All calculations were performed using the periodic boundary conditions by utilizing the IMAGE facility in CHARMM. Through the use of the adopted basis Newton–Raphson method,⁶⁰ the energy of the silica slabs were minimized. The minimum energy structures were obtained by repeated melting between 300 and 500 K and quenching to 50 K. Several cycles of heating and cooling resulted in relaxation of the surface hydroxyl groups; however, the relaxation did not lead to any reconstruction of the surfaces. This first step is important for studying water adsorption, as water was introduced on relaxed silica surfaces.

IV. Results and Discussion

We present the results of H-bonding patterns between the nearest-neighbor hydroxyl groups (intrasurface H-bonding) and water adsorption studies on 40 hydroxylated β -cristobalite surfaces. Sections A and B present the results and discussion of intrasurface H-bonding and water adsorption on the surfaces, respectively.

IV. A. Intrasurface H-Bonding. All 40 unique β -cristobalite surfaces are quantified by their percentage of Q^2 and Q^3 centers, and the results are listed in Table 1. An average over the surfaces listed in Table 1 indicates that the Q^2 centers are less abundant with a 23% abundance as compared to 77% of the Q^3 centers. This simple estimate is in accordance with the experimentally determined 15–30% Q^2 abundance for β -cristobalite.^{29,30,32} A frequency distribution of the Q^2 percentage abundance data for the family of 40 surfaces is shown in Figure 1. A striking feature of the data in Table 1 and Figure 1 is the uniqueness of the {100} surface in terms of the high percentage of Q^2 centers. Given that β -cristobalite does not have a preferred cleavage plane,⁴² we conclude that the commonly studied {100} surface is atypical and is not representative of experimentally investigated surfaces of polycrystalline or amorphous silica.

**Figure 1.** The frequency distribution of the number of β -cristobalite surfaces versus the percentage abundance of Q^2 centers.

The ability of a hydroxylated surface to form hydrogen bonds within the surface is controlled by the oxygen–oxygen (OO) distance. A distance of less than 3.2 Å allows for H-bond formation. In addition, the O–H distance must be less than 2.5 Å and the O–H–O angle greater than 90°. By using these simple geometric conditions, the propensity to form H-bonds within a surface can be calculated.

We first benchmark our results for the {100} surface with ab initio results available in the literature.³⁹ The average OO distance reported by Yang et al.³⁹ is 2.82 Å as compared to values of 2.80 Å and 2.71 Å that were obtained using the CHARMM and FG potentials, respectively. The lattice parameters for the calculations are shown in Table 2, and compare well with the experimental and previous theoretical data.^{39,61} Figure 2 shows the optimized surface with H-bonds between the neighboring Q^2 centers. The two hydroxyl groups at the same Q^2 center (geminal hydroxyls) do not interact with each other in agreement with the previous results obtained by Yang et al.³⁹ Each Q^2 center forms two H-bonds with its neighbors through its two hydroxyl groups with the oxygen of one hydroxyl acting as a H-donor and the other one acting as an acceptor. The donor oxygen atom and its hydrogen atom and the acceptor oxygen atom lie in plane parallel to the surface while the hydrogen atom of the acceptor oxygen atom is projected out-of-the-plane of the surface. The configuration of the hydrogen atoms projected out-of-the plane of the surface plays a major role in water adsorption on the surface and will be discussed in the next section. The overall level of agreement between the previous ab initio studies and the work presented here for the {100} family of surfaces validates the use of FG and CHARMM potentials and further extension of these methods for studies of the remaining sets of surfaces.

There are nine crystallographic planes with 100% Q^3 centers, but they differ from each other in the distribution of these centers on the surface. Figures 3 and 4 show the optimized {111} and {011} β -cristobalite surfaces, both having hydroxyl groups at Q^3 centers. In the {111} surface, all hydroxyls are in the same plane, whereas the {011} surface has a stepwise arrangement of the hydroxyl groups. Along the {111} surface, the Q^3 centers are uniformly spaced following a $-(Q^3-O-Q^4-O)-$ template, as shown in Figure 3. We label this type of Q^3 center as Q^{3A} . The average nearest-neighbor OO distance between the hydroxyl groups is greater than 5.1 Å using both potentials, as shown in Table 3, and is too long to allow intrasurface H-bonds. The

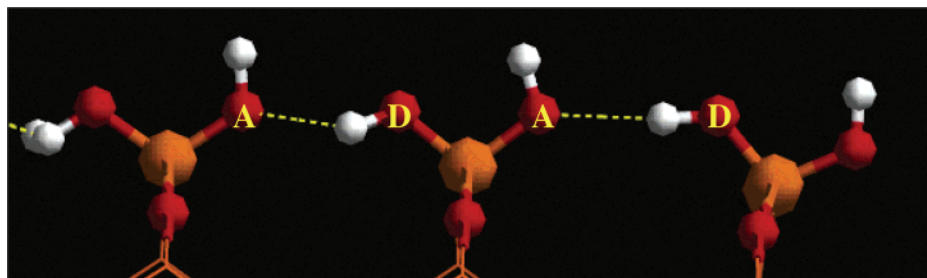


Figure 2. The $\{100\}$ hydroxylated β -cristobalite surface showing H-bonding (in yellow dashed line) between neighboring Q^2 centers. The Si, O, and H-atoms are shown in orange, red, and white colors, respectively. The donor oxygen atom is denoted by **D**, and the acceptor oxygen atom is shown by **A**.

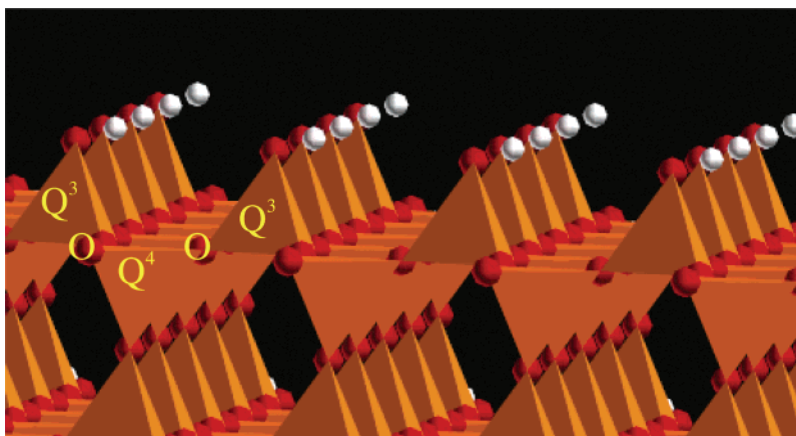


Figure 3. The $\{111\}$ β -cristobalite surface showing the orientation of the hydroxyl groups and lack of H-bonding between the Q^{3A} centers. The SiO_4 groups are represented by the tetrahedrons, and the O and H-atoms are shown as red and white balls, respectively. As a guide to the eye, the $-(Q^3-O-Q^4-O)-$ repeat unit is labeled.

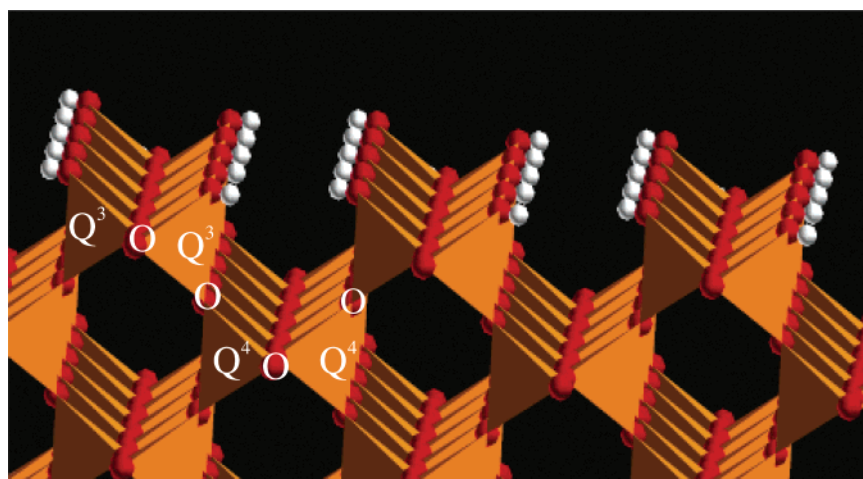


Figure 4. Optimized hydroxylated $\{011\}$ β -cristobalite surface with stepwise arranged Q^{3B} centers resulting in lack of H-bonding. Each tetrahedron represents the SiO_4 group with Si atom at the center, and O and H-atoms are shown in red and white colors, respectively. As a guide to the eye, the $-(Q^3-O-Q^3-O-Q^4-O-Q^4-O)-$ template is labeled.

$\{011\}$ surface has an asymmetric arrangement around the Q^3 centers with a $-(Q^3-O-Q^3-O-Q^4-O-Q^4-O)-$ repeat unit in which the Q^3-O-Q^3 subunit is separated from the Q^4-O-Q^4 subunit by an oxygen atom. We label this arrangement of Q^3 centers as Q^{3B} . As a result, the Q^3 centers have two nearest-neighbor O-O distances, neither of which is sufficiently short for the formation of intrasurface hydrogen bonds. The OO distances obtained using both the CHARMM and FG potentials are listed in Table 3. For Q^{3A} centers, the lack of H-bonding can be attributed to the large separation between the Q^3 centers. For the Q^{3B} centers, in addition to the large distance the hydroxyl groups do not lie in the same plane. This topological difference

in the arrangement has significant effects on the nature of the water adsorption on these surfaces.

The other surfaces with 100% Q^3 centers are further classified in Table 1 as A, B, or AB based on the type of Q^3 centers. The AB classification is for the surfaces that have both A and B type of Q^3 centers. The remaining surfaces have both Q^2 and Q^3 sites, and depending on the abundance of Q^2 sites, each surface is qualitatively different from the other in terms of H-bonding.

Out of the 40 surfaces studied, 25 surfaces with Q^3 site percentages greater or equal to 78% do not show H-bonding because the Q^3 sites are topographically too far apart with an

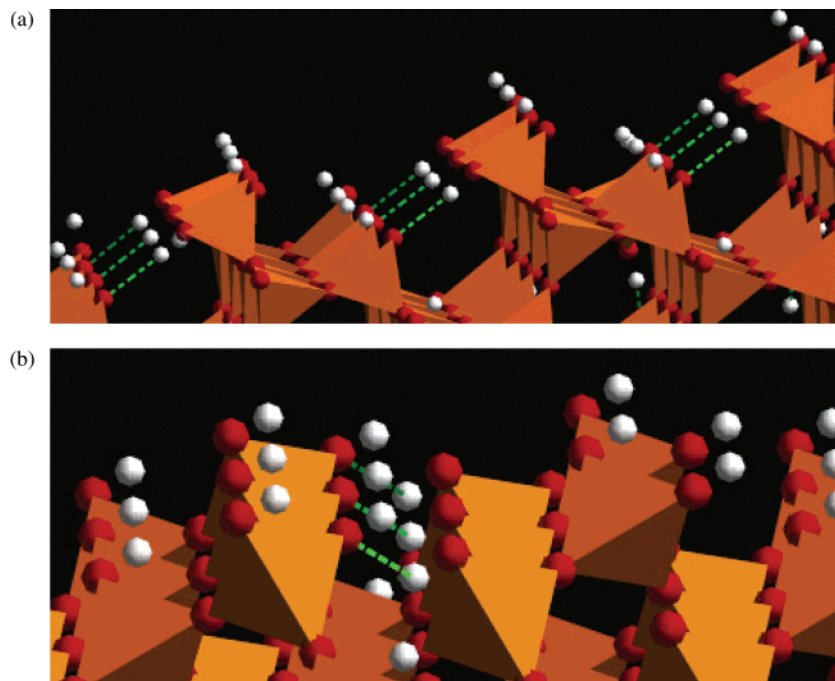


Figure 5. β -cristobalite surfaces showing H-bonding pattern in (a) $\{113\}$ plane with a Q^2/Q^3 site ratio of 1:3 and a ladderlike surface arrangement forming hydrogen bond bridges (green dashed lines) between the O-atom (red) of the hydroxyl at Q^3 site and the H-atom (white) of one of the two hydroxyls at the Q^2 site and (b) $\{013\}$ plane with 1:1 ratio of Q^2/Q^3 sites. The bulk of the crystal is represented as a tetrahedron of SiO_4 groups, and the O and H-atoms are shown in red and white-colored balls, respectively.

average OO distance of 4.2 Å. The remaining 14 surfaces show H-bonding, and in Table 4 the average O–H bond distances and the percentage of number of H-bonds per hydroxyl group are listed. The data in Table 4 show that the surfaces with a low percentage of H-bonds have weaker and longer H-bonds. This observation can be attributed to the corrugation of the surface. Figure 5 shows the H-bonding pattern for two surfaces: the $\{113\}$ surface that has 66% of the hydroxyls H-bonded and a 1:3 ratio of Q^2/Q^3 sites and the $\{013\}$ surface that has 30% H-bonded hydroxyls with a 1:1 ratio of Q^2/Q^3 sites. The $\{113\}$ surface shows an ordered pattern and H-bonds are formed between the oxygen atom of the Q^3 site and the H-atom of one of the hydroxyl groups at the Q^2 site. The average O–H bond distance is 2.18 Å for the $\{113\}$ surface and 2.27 Å for the $\{013\}$ surface. This analysis indicates that the topology of the surface determines the strength of the H-bonds.

IV. B. Water Adsorption. The adsorption of water on the surface is quantified by calculating the adsorption energy

$$E_{\text{ads}} = -(E_{\text{total}} - E_{\text{surf}} - nE_w)/n \quad (8)$$

where E_{total} is the total energy of the system (silica surface with adsorbed water molecules), E_{surf} is the energy of the optimized surface, E_w is the energy of the isolated water molecule, and n is the number of adsorbed molecules. A monolayer of adsorbed water on fully relaxed hydroxylated surfaces was investigated.

The results indicate that the surfaces with ordered topology and hydroxyl groups in planes parallel to the surface, for example, the $\{100\}$ and $\{111\}$ hydroxylated surfaces of β -cristobalite, have accessible hydroxyl groups that can adsorb water molecules through H-bonds. In contrast, the surfaces that are corrugated or have less-ordered topology do not have the hydroxyls in one plane to adsorb water effectively to form a stable monolayer. Depending on the local topology of the corrugation, the surface can adsorb single water molecules with very different adsorption energies and stabilities.

TABLE 5: Adsorption Energies for Cristobalite Surfaces

surface	E_{ads} (meV)			
	FG	CHARMM	ref 39	ref 22
$\{100\}$	529	478	502	
$\{111\}$	484	461		
Crystalline (150 K)				560
Crystalline (500 K)				539

The $\{100\}$ surface with 100% Q^2 sites has geminal hydroxyl groups in a plane parallel to the surface and forms a stable tessellated H-bond network. Ab initio methods have been used extensively to investigate water adsorption on the (100) plane,³⁹ and we use this data to benchmark the MD calculations in this work. Table 5 provides the adsorption energies for the $\{100\}$ and $\{111\}$ surfaces using both the FG and CHARMM potentials. The adsorption energy values for both potentials are in agreement with the previously reported ab initio value³⁹ for the $\{100\}$ and this allows us to extend the water adsorption studies to the other 39 surfaces and explore the other less-studied surfaces. The experimental water adsorption data on cristobalite²² at 150 and 500 K and under equilibrium pressure are in very good agreement with the results obtained in the present work.

Depending on the topography, the 100% Q^{3A} surfaces show differences in water adsorption. The $\{111\}$ surface adsorbs water to form closed ring structures using two H-bonds with the surface hydroxyl groups, bridging the neighboring Q^{3A} centers. The adsorption energy for the $\{111\}$ surface using the FG potential is 484 meV per water molecule, 45 meV lower than the value for the $\{100\}$ surface. The CHARMM potential shows a decrease of 17 meV in adsorption energy for the $\{111\}$ surface. Both the potentials are in qualitative agreement that water is less strongly adsorbed on the $\{111\}$ surface as compared to the $\{100\}$ surface. Figure 6 shows the adsorbed water monolayers on $\{111\}$ from three different perspectives. The H-bond distance between the O-atom of adsorbed water and H-atom of the surface (O_w-H_s) is 1.81 Å, and the surface oxygen atom to hydrogen atom of water (O_s-H_w) distance is 1.95 Å. The $\{334\}$

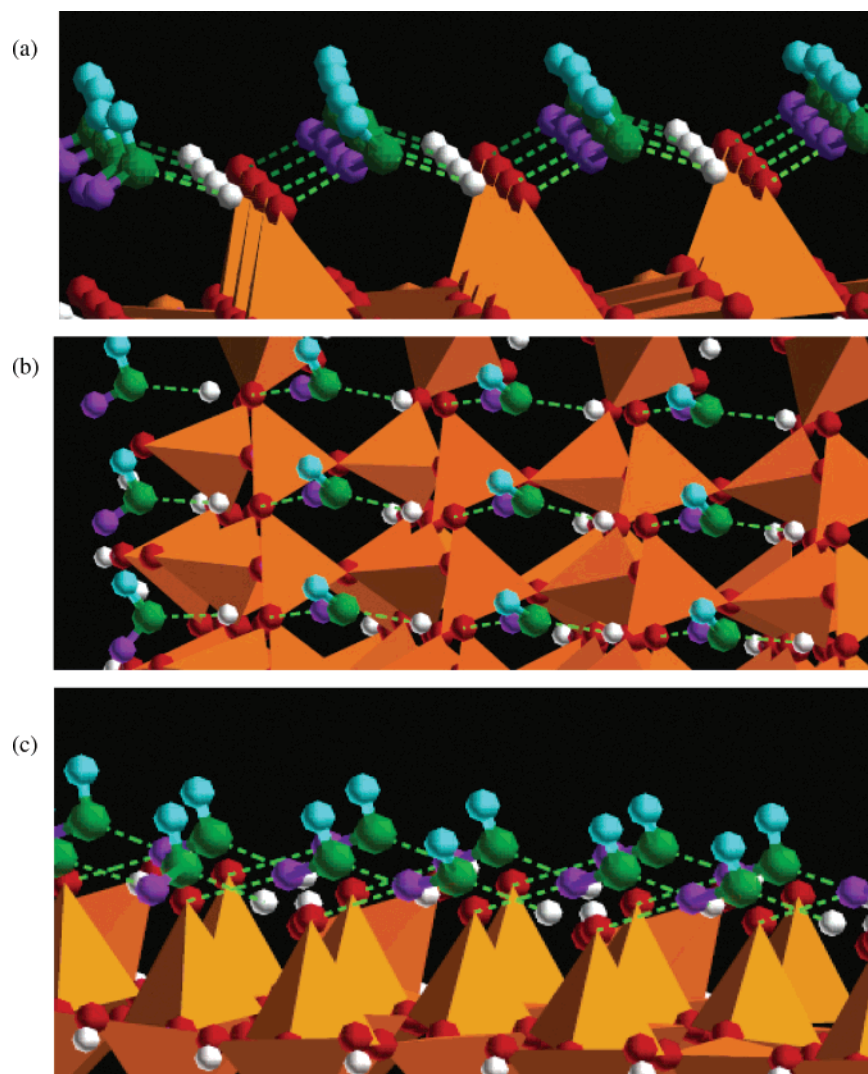


Figure 6. Hydroxylated $\{111\}$ β -cristobalite surface with adsorbed monolayer of water, forming linear chains pattern. Each water molecule is held between the neighboring Q^3 centers by two H-bonds (dashed green lines). The bulk of the crystal is represented as a tetrahedron of SiO_4 groups, and the surface hydroxyls are shown in colored balls (with O and H-atoms in red and white, respectively). The O-atoms (green) of adsorbed water act as a donor–acceptor, donating one of the H-atoms (purple), whereas the second H-atom (light blue) is projected out-of-the-plane of the surface. In panel (a) the ring, (b) the linear chains, and (c) the network perspectives of the surface water interaction are shown.

surface is similar to the $\{111\}$ surface and consequently exhibits a similar H-bonding pattern with an O_W-H_S distance of 1.79 Å and an O_S-H_W distance of 1.91 Å. The shorter O_W-H_S bond compared to O_W-H_S bonds for water adsorbed to both $\{111\}$ and $\{334\}$ shows that the surface oxygen atom is a better donor than the oxygen atom of the water molecule.

On the other hand, the pure Q^{3B} surfaces and the surfaces with a mix of Q^{3A} and Q^{3B} sites do not show a tessellated network of adsorbed water overlayers. Since all these are pure Q^3 surfaces, this difference in water adsorption property can be attributed to the corrugated topography of the surface. These surfaces adsorb water locally depending strongly on the relative abundance and accessibility to the neighboring hydroxyl groups. X-ray reflectivity experiments on quartz surfaces have shown that smoothness of the surface was crucial in the formation of water monolayers.³⁶ A similar dependence on the surface topology is exhibited by the surfaces with a mix of Q^3 and Q^2 sites. Figure 7 shows examples of isolated water adsorption sites on the $\{113\}$ and $\{013\}$ surfaces. The water molecules are held by hydrogen bonds to the surface but unlike the $\{100\}$ or $\{111\}$ surface (Figures 2 and 6, respectively) there is no tessellation.

V. Implications

The differing structures of these silica–water interfaces may have direct implications for the corrosion of silica-based materials and for the weathering of silicates in the natural environment. Zhao et al.⁶² studied the related phenomenon of chemical reactivity of silica surfaces and concluded that silylation of high-surface area amorphous silicas by trimethylchlorosilane dominantly occurs at isolated Q^3 surface sites, hypothetically due to the thermodynamic barrier disrupting H-bonding networks on the surface. This hypothesis is supported by the observation made by Kawai et al. that regions exhibiting extensive intrasurface H-bonding on aluminum containing zeolites precluded silanization.⁶³ Similarly, Washton et al.⁶⁴ have observed that the number of surface hydroxyl sites on low-surface area aluminosilicates silylated by (3,3,3-trifluoropropyl) dimethylchlorosilane were proportional to the dissolution rates of natural and man-made glasses. Given this hypothesis and observations, we propose that the dissolution rate of β -cristobalite will be dominated by surfaces with a larger percentage of isolated Q^3 silanols groups. Although the percentages of surfaces and the relative ratios of various Q^i sites will be

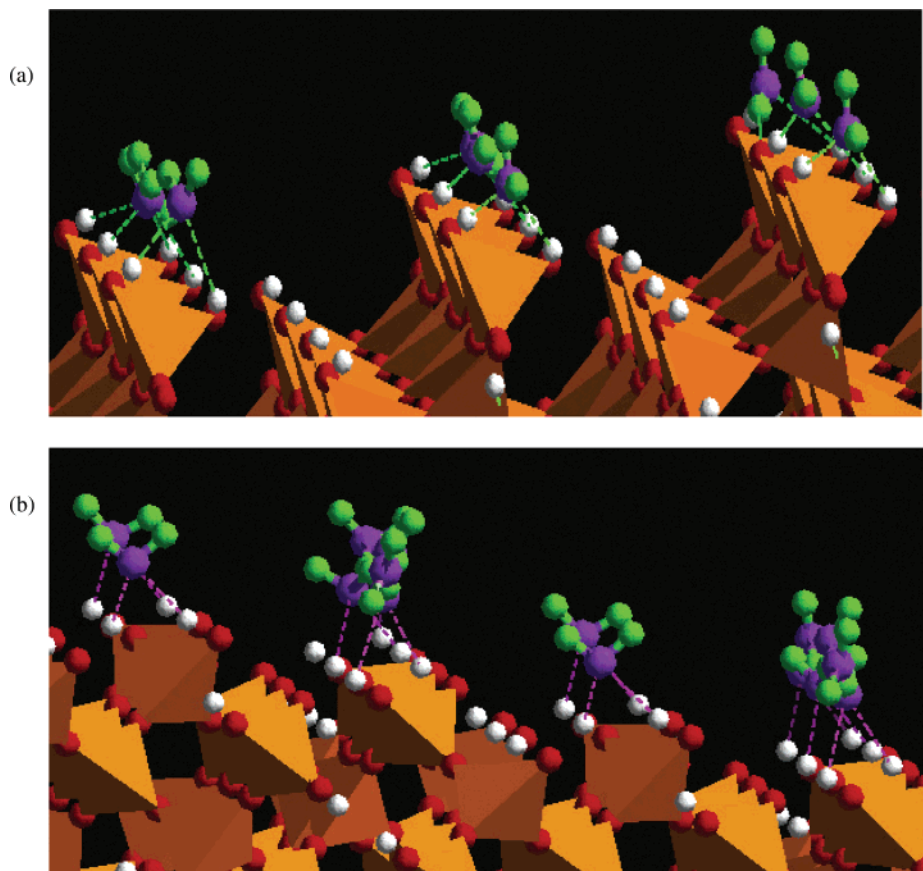


Figure 7. β -cristobalite surfaces showing localized sites of water adsorption on (a) $\{113\}$ and (b) $\{013\}$ planes. The water molecules are held by H-bonds (dashed lines) between the O-atom of water (purple) and the H-atom (white) of the surface. The H-atoms of water are shown in green color. The bulk of the crystal is represented as a tetrahedron of SiO_4 groups, and the surface hydroxyls are shown in colored balls (with O and H-atoms in red and white, respectively).

different on other forms of silica, this interpretation is likely to be valid for all crystalline forms of silica if we assume that the thermodynamics of the silica–water interface do not change significantly. One can also speculate that this phenomenon will influence silica crystal-growth kinetics as well because the interfacial energy is critical as nanoparticles form crystal-growth nuclei.^{65,66}

With regard to the human health aspects of inhaled silica particles, Fubini et al.²² have shown that the energy of H_2O adsorption onto β -cristobalite is related to the cytotoxicity of the cristobalite. This study has identified the surface sites and types of crystal surfaces that are likely to have the greater H_2O adsorption energy that is related to the cytotoxic particles. Combined with the prediction that these silica–water interface reactions can lead to the production of OH-radicals,⁶⁷ the source of silica cytotoxicity becomes more clear. The potential OH-radical generation capability of silica particles in general could be derived from similar analyses of the possible surfaces of a given crystal form. More hydrophobic particles with a predominance of Q^3 surface sites can be designed to limit the potential human health impacts of crushed and nanoparticulate silicas used in industry.

VI. Summary

This work presents a study of β -cristobalite surfaces along 40 unique crystallographic planes using molecular dynamics simulations. We used two empirical potential energy functions to study the surface properties of intrasurface H-bonding and water adsorption. Our results using empirical potentials on

hydroxylated $\{100\}$ β -cristobalite surface agreed with the previous ab initio studies, and we extended our work to other less-explored and uncharacterized surfaces. We find that the polymeric states of the surface silicon atoms and the topological features of the arrangement of the surface hydroxyls are crucial in describing the surface properties along any crystallographic plane. On average over all the crystallographic planes studied, Q^3 centers are abundant in the ratio of 3:1 as compared to Q^2 centers. We found nine crystallographic planes with pure Q^3 centers and only one with pure Q^2 centers; the rest of the surfaces are a combination of Q^2 and Q^3 centers.

Our studies show that the $\{100\}$ surface, the most commonly examined β -cristobalite surface theoretically, is different from other β -cristobalite surfaces. The $\{100\}$ surface is unique in its propensity of Q^2 sites; it forms very stable intrasurface H-bonds and tessellation patterns with the adsorbed water monolayer unlike any of the other surfaces. We report two types of pure Q^3 surfaces, $\text{Q}^{3\text{A}}$ and $\text{Q}^{3\text{B}}$, based on the surface topology. Neither $\text{Q}^{3\text{A}}$ and $\text{Q}^{3\text{B}}$ show intrasurface H-bonds, but the $\{111\}$ $\text{Q}^{3\text{A}}$ surface exhibits an ordered water adsorption pattern whereas the $\{011\}$ $\text{Q}^{3\text{B}}$ surface does not. Water adsorption is mainly dependent on the topology of the surface, and ordered pattern $\{100\}$ and $\{111\}$ surfaces form stable monolayers. Stepped and corrugated surfaces have no uniform hydroxyl group arrangement and do not adsorb water effectively.

We find the quest to understanding water adsorption technically important for silica-based chemistry as it has high natural abundance and has large-scale industrial applications. This study helps us understand the microscopic differences in crystalline

surfaces using theoretical methods that are computationally affordable and practical for systems with large numbers of atoms.

Acknowledgment. This work has been supported by the National Science Foundation NSF under Grant Number CHE-0535656. J.D.K. and N.M.W. acknowledge the support of the Penn State Center for Environmental Kinetics Analysis, NSF Grant Number CHE-0431328.

References and Notes

- (1) Ostroverkhov, V.; Waychunas, G. A.; Shen, Y. R. *Chem. Phys. Lett.* **2004**, *386*, 144.
- (2) Ostroverkhov, V.; Waychunas, G. A.; Shen, Y. R. *Phys. Rev. Lett.* **2005**, *94*, 046102.
- (3) Li, I.; Bandara, J.; Shultz, M. J. *Langmuir* **2004**, *20*, 10474.
- (4) McCarthy, D. W.; Mark, I. E.; Schaefer, D. W. *J. Polym. Sci., Part B* **1998**, *36*, 1167.
- (5) Rignanes, G.-M.; Charlier, J.-C.; Gonze, X. *Phys. Chem. Chem. Phys.* **2004**, *6*, 1920.
- (6) Rignanes, G.-M.; Vita, S. D.; Charlier, J.-C.; Gonze, X.; Car, R. *Phys. Rev. B* **2000**, *61*, 13250.
- (7) Murashov, V. V. *J. Chem. Phys. B* **2005**, *109*, 4144.
- (8) Adair, J. H.; Cho, S. B.; Bell, N. S.; Perrotta, A. J. *J. Dispersion Sci. Technol.* **2001**, *22*, 143.
- (9) Xiao, Y.; Lasaga, A. C. *Geochim. Cosmochim. Acta* **1996**, *60*, 2283.
- (10) Xiao, Y.; Lasaga, A. C. *Geochim. Cosmochim. Acta* **1994**, *58*, 5379.
- (11) Nalewajski, R. F.; Koster, A. M.; Bredow, T.; Jug, K. *J. Mol. Catal.* **1993**, *82*, 407.
- (12) Fahmi, A.; Minot, C. A. *Surf. Sci.* **2006**, *304*, 343.
- (13) Henderson, M. A. *Langmuir* **1996**, *12*, 5093.
- (14) Bullard, J. W.; Cima, M. J. *Langmuir* **2006**, *22*, 10264.
- (15) Miffliin, A. L.; Konek, C.; Al-Abadleh, H.; Geiger, F. M. *Geochim. Cosmochim. Acta* **2004**, *68*, A163.
- (16) Konek, C. T.; Illg, K. D.; Al-Abadleh, H. A.; Voges, A. B.; Yin, G.; Musorrafiti, M. J.; Schmidt, C. M.; Geiger, F. M. *J. Am. Chem. Soc.* **2005**, *127*, 15771.
- (17) Brantley, S. L.; Crane, S. R.; Crerar, D. A.; Hellmann, R.; Stallard, R. *Geochim. Cosmochim. Acta* **1986**, *50*, 2349.
- (18) Gratz, A. J.; Bird, P.; Quiro, G. B. *Geochim. Cosmochim. Acta* **1990**, *54*, 2911.
- (19) Gratz, A. J.; Bird, P. *Geochim. Cosmochim. Acta* **1993**, *57*, 977.
- (20) Gautier, J.-M.; Oelkers, E. H.; Schott, J. *Geochim. Cosmochim. Acta* **2001**, *65*, 1059.
- (21) Castagliola, M.; Tellier, C. R.; Vaterkowski, J. L. *J. Mater. Sci.* **1986**, *21*, 3551.
- (22) Fubini, B.; Zanetti, G.; Altilia, S.; Tiozzo, R.; Lison, D.; Saffiotti, U. *Chem. Res. Toxicol.* **1999**, *12*, 737.
- (23) Bunker, B. C.; Tallant, D. R.; Headley, T. J.; Turner, G. L.; Kirkpatrick, R. J. *Phys. Chem. Glasses* **1988**, *29*, 106.
- (24) Trinh, T. T.; Jansen, A. P. J. *J. Phys. Chem. B* **2006**, *110*, 23099.
- (25) Engelhardt, G.; Jancke, H.; Hoebbel, D.; Weiker, W. *Z. Chem.* **1974**, *14*, 109.
- (26) Engelhardt, G.; Zeigan, D.; Jancke, H.; Hoebbel, D.; Weiker, W. *Z. Anorg. Allg. Chem.* **1975**, *418*, 17.
- (27) Harris, R. K.; Knight, C. T. *G. J. Mol. Struct.* **1982**, *78*, 273.
- (28) Harris, R. K.; Newman, R. H. *J. Chem. Soc., Faraday Trans. 2* **1977**, *73*, 1204.
- (29) Léonardelli, S.; Facchini, L.; Fretigny, C.; Tougne, P.; Legrand, A. P. *J. Am. Chem. Soc.* **1992**, *114*, 6412.
- (30) Tuel, A.; Hommel, H.; Legrand, A. *Langmuir* **1990**, *6*, 770.
- (31) Sindrof, D. W.; Maciel, G. E. *J. Phys. Chem.* **1982**, *86*, 5208.
- (32) Sindrof, D. W.; Maciel, G. E. *J. Am. Chem. Soc.* **1983**, *105*, 1487.
- (33) Marrow, B. A.; McFarlan, A. J. *J. Phys. Chem.* **1992**, *96*, 1395.
- (34) Voort, P. V. D.; Gillis-D'Hamers, I.; Vansant, E. F. *J. Chem. Soc., Faraday Trans.* **1990**, *86*, 3751.
- (35) Voort, P. V. D.; Gillis-D'Hamers, I.; Vrancken, K. C.; Vansant, E. F. *J. Chem. Soc., Faraday Trans.* **1991**, *87*, 3899.
- (36) Schlegel, M. L.; Nagy, K. L.; Fenter, P.; Sturchio, N. C. *Geochim. Cosmochim. Acta* **2002**, *66*, 3037.
- (37) Odelius, M.; Bernasconi, M.; Parrinello, M. *Phys. Rev. Lett.* **1997**, *78*, 2855.
- (38) Yang, J.; Wang, E. G. *Phys. Rev. B* **2006**, *73*, 035406.
- (39) Yang, J.; Meng, S.; Xu, L. F.; Wang, E. G. *Phys. Rev. Lett.* **2004**, *92*, 146102.
- (40) Vigné-Maeder, F.; Sautet, P. *J. Phys. Chem. B* **1997**, *101*, 8197.
- (41) Lopes, P. E. M.; Murashov, V.; Tazi, M.; Demchuk, E. A. D.; MacKerell, J. J. *J. Phys. Chem. B* **2006**, *110*, 2782.
- (42) Nesse, W. D. *Introduction to Mineralogy*; Oxford University Press: New York, 2000.
- (43) Feuston, B. P.; Garofalini, S. H. *J. Chem. Phys.* **1988**, *89*, 5818.
- (44) Rustad, J. R.; Hay, B. P. *Geochim. Cosmochim. Acta* **1995**, *59*, 1251.
- (45) Feuston, B. P.; Garofalini, S. H. *J. Phys. Chem.* **1990**, *94*, 5351.
- (46) Feuston, B. P.; Garofalini, S. H. *Chem. Phys. Lett.* **1990**, *170*, 264.
- (47) Martin, G.; Garofalini, S. H. *J. Non-Cryst. Solids* **1994**, *171*, 68.
- (48) Garofalini, S. H.; Martin, G. *J. Phys. Chem.* **1994**, *98*, 1311.
- (49) Litton, D. A.; Garofalini, S. H. *J. Appl. Phys.* **2001**, *89*, 6013.
- (50) Brooks, B. R.; Bruccoleri, R. E.; Olafson, B. D.; States, D. J.; Swaminathan, S.; Karplus, M. *J. Comp. Chem.* **1983**, *4*, 187.
- (51) MacKerell, A. D., Jr.; Brooks, B.; Brooks, C. L., III; Nilsson, L.; Roux, B.; Won, Y.; Karplus, M. *CHARMM: The Energy Function and Its Parameterization with an Overview of the Program*; John Wiley and Sons: Chichester, England, 1998; Vol. 1.
- (52) Ha, S. N.; Giammona, A.; Field, M.; Brady, J. W. *Carbohydr. Res.* **1988**, *180*, 207.
- (53) MacKerell, A. D., Jr.; Wiórkiewicz-Kuczera, J.; Karplus, M. *J. Am. Chem. Soc.* **1995**, *117*, 11946.
- (54) MacKerell, A. D., Jr.; Bashford, D.; Bellott, M.; Dunbrack, R. L., Jr.; Evanseck, J. D.; Field, M. J.; Fischer, S.; Gao, J.; Guo, H.; Ha, S.; Joseph-McCarthy, D.; Kuchnir, L.; Kuczera, K.; Lau, F. T. K.; Mattos, C.; Michnick, S.; Ngo, T.; Nguyen, D. T.; Prodhom, B.; Reiher, W. E., III; Roux, B.; Schlenkrich, M.; Smith, J. C.; Stote, R.; Straub, J.; Watanabe, M.; Wiórkiewicz-Kuczera, J.; Yin, D.; Karplus, M. *J. Phys. Chem.* **1998**, *102*, 3586.
- (55) Stillinger, F. H.; Weber, T. A. *Phys. Rev. B* **1985**, *31*, 5262.
- (56) Stillinger, F. H.; Rahman, A. *J. Chem. Phys.* **1978**, *68*, 66.
- (57) *Cerius² Modeling Environment*, Release 4.0; Accelrys Inc.: San Diego, CA, 1999.
- (58) Ashcroft, N. W.; Mermin, N. D. *Solid State Physics*; Saunders College Publishing: Fort Worth, TX, 1976.
- (59) Jorgensen, W. L.; Chandrasekhar, J.; Madura, J. D.; Impey, R. W.; Klein, M. L. *J. Chem. Phys.* **1983**, *79*, 926.
- (60) Chu, J.-W.; Trout, B. L.; Brooks, B. R. *J. Chem. Phys.* **2003**, *119*, 9563.
- (61) Wright, A. F.; Leadbetter, A. J. *Philos. Mag.* **1975**, *31*, 1391.
- (62) Zhao, X. S.; Lu, G. Q.; Whittaker, A. K.; Millar, G. J.; Zhu, H. Y. *J. Phys. Chem. B* **1997**, *101*, 6525.
- (63) Kawai, T.; Tsutsumi, K. *Colloid Polym. Sci.* **1998**, *276*, 992.
- (64) Washton, N. M.; Brantley, S. L.; Mueller, K. T. *Geochim. Cosmochim. Acta*, submitted for publication, 2007.
- (65) Levchenko, A. A.; Li, G. S.; Boerio-Goates, J.; Woodfield, B. F.; Navrotsky, A. *Chem. Mater.* **2006**, *18*, 6324.
- (66) Boerio-Goates, J.; Li, G. S.; Li, L. P.; Walker, T. F.; Parry, T.; Woodfield, B. F. *Nano Lett.* **2006**, *6*, 750.
- (67) Narayanasamy, J.; Kubicki, J. D. *J. Phys. Chem. B* **2005**, *109*, 21796.